Homogeneous Palladium Nanoparticles Surface Hosts Catalyzed Reduction of the Chromophoric Azo (–N=N–) Group of Dye, Acid Orange 7 by Borohydride in Alkaline Media

RANENDU SEKHAR DAS,[1] BULA SINGH,[2] ARABINDA MANDAL,[3] RUPENDRANATH BANERJEE,[1] SUBRATA MUKHOPADHYAY[1]

[1]*Department of Chemistry, Jadavpur University, Kolkata* 700 032, *India*

[2]*Department of Chemistry, Visva-Bharati, Santiniketan* 731 235, *India*

[3]*Department of Chemistry, Haldia Government College, Purba Medinipur* 721 657, *India*

Received 24 April 2014; revised 10 September 2014; accepted 10 September 2014

DOI 10.1002/kin.20883
Published online 20 October 2014 in Wiley Online Library (wileyonlinelibrary.com).

ABSTRACT: In alkaline media, well-characterized gelatin-stabilized palladium (GPd) nanoparticles catalyze the reduction of the azo group containing pollutant dye, Acid Orange 7 (AO7) by sodium borohydride ($NaBH_4$) to 1-amino-2-napthol and sulfanilic acid. Kinetic observations and detailed FTIR studies suggests that the reaction follows Langmuir–Hinshelwood kinetic model, where during the reaction both AO7 and borohydride are adsorbed on the GPd surface. Plots of $\ln k_o$ versus $\ln[AO7]$ or $\ln[NaBH_4]$ show that the order of reaction with respect to AO7 and $NaBH_4$ remains almost same over different molar ratios of $[NaBH_4]/[AO7]$. The catalyzed reaction shows an initial induction period (t_0) due to a surface-restructuring process of GPd nanoparticles, and ($1/t_0$) can be defined as the rate of surface restructuring. The activation energy of the catalyzed reaction and energy of the surface-restructuring process of GPd are estimated as 22 ± 3 and 25 ± 7 kJ M^{-1}, respectively. © 2014 Wiley Periodicals, Inc. Int J Chem Kinet 46: 746–758, 2014

Correspondence to: R. S. Das; e-mail: ranendu147@gmail.com

Supporting Information is available in the online issue at www.wileyonlinelibrary.com.

INTRODUCTION

Since the accidental discovery of the first synthetic dye, Mauveine, in the middle of 19th century [1], numerous

other dyes of different classes had been synthesized and commercialized in accord with the huge usage in different industries such as textiles, leather, and paper [2–6]. Among different class of dyes, azo dyes, which consists of one or more azo groups (–N=N– bond), alone accounts for almost half of the synthetic dyestuffs used in industries [7–9].

The escalating use of dyestuffs became alarming when it was found that a large amount of colorants used for dyeing is released through the sewage water from the industries [7–9]. Since except one single compound (4,4′-dihydroxyazo-benzene), naturally occurring products do not contain the azo group [10], it is expected that the released azo dye contaminants will be harmful both for human and for all other living beings [11–14]. It has been found that azo dyes are relatively persistent pollutants because under aerobic conditions they are hard to biodegrade [9,15–18] compared to their reduced amine products [13]. Consequently, in many countries, the release of dye-contaminated effluents in environment is highly prohibited and the subject has long been a topic of debate from the standpoints of socio-political views.

To confront this major challenge to degrade these wastewater pollutants, different biochemical and physiochemical techniques, mainly fungal and bacterial decomposition [19–21], enzymatic degradation [22], coagulation [23,24], adsorption [25–27], photocatalytic oxidation [28–30], Fenton oxidation [30–33], advanced oxidation processes [34,35], and chemical reduction [36–42], have been frequently employed to decolorize and scavenge these colorants from waste water.

Since most of the biochemical and biophysical processes require a large amount of adsorbents along with other means, such as intricate reactors and intensive power supply [9,38], researchers have put much emphasis on the chemistry of different metals or metal composites (containing mostly iron, nickel, copper, etc.) mediated reduction of azo dyes [36–42]. Although these reduction processes are efficient but one serious concern lies in the usual practice of large usage of metal dosages, which generate metal sludge as secondary wastes [31]. In search of a more suitable process, therefore, we have turned our focus on the use of noble metal nano-like palladium, which under aerobic condition, even in the presence of astoundingly small concentration (10^{-10} M, vide infra), catalyzes the reduction of an azo dye, Acid Orange 7 (AO7, 4-(2-hydroxy-1-naphthylazo)benzenesulfonic acid) by sodium borohydride ($NaBH_4$) to 1-amino-2-napthol and sulfanilic acid at ambient conditions [13,43,44].

In this study, we have developed a quick and easy method of synthesis of stable homogeneous gelatin-capped palladium nanoparticles (GPd) and studied the detailed kinetics of the catalyzed reduction of AO7 by sodium borohydride in aqueous alkaline media ([NaOH] = 0.1–0.5 M) keeping in view the facile use of the nanoparticles-catalyzed reaction to remove the harmful azo dye remnants from the effluents.

EXPERIMENTAL

Materials

Palladium(II) chloride (Aldrich, USA), sodium citrate dihydrate (Rankem, India), gelatin (Merck, Germany), Acid Orange 7 (Aldrich, USA), sodium borohydride (Merck, Germany), sodium nitrate (Merck, Germany), and sodium hydroxide (SRL, India) were used as received. Milli-Q water and doubly distilled water was used for the preparation of nanoparticles and kinetic experiments, respectively. All the other chemicals used were of analytical grade.

Preparation of Gelatin-Stabilized Palladium Nanoparticles (GPd)

Palladium nanoparticles had a substantial history of synthesis and usage [45]. Here, an easy and one-pot synthetic procedure was developed for the preparation of gelatin-stabilized palladium nanoparticles (GPd). Palladium nanoparticles were prepared from the precursor Pd(II) ions by the reduction with trisodium citrate. Citrate ions reduce Pd(II) to Pd(0), and then through the nucleation process Pd(0) forms palladium nanoparticles. Citrate ions also primarily stabilize the palladium nanoparticles electrostaticlly, forming an electrical double layer at the particle interfaces [46]. Since the interaction between the nanoparticles and the citrate ions is relatively weak, aqueous gelatin was added to the preformed palladium nanoparticles for better and prolonged stabilization. Gelatin is a common, naturally occurring denatured product of collagen, which is well known as a stabilizing agent. Moreover, it does not react with the reactants or passivate the nanoparticle surfaces [47–49].

GPd was prepared by following the procedure: 50 mL of an aqueous $PdCl_2$ solution (2.5×10^{-4} M) was heated to boiling with vigorous stirring. Then 2 mL of 1% (w/v) aqueous trisodium citrate solution was added to the solution, and the solution was allowed to boil for 1 h with vigorous stirring. The formation of the Pd nanoparticles can be followed by the appearance of yellow color in the solution. Then 5 mL of 1% (w/v) aqueous gelatin solution was added to the preformed Pd nanoparticles solution and the boiling was

continued for another 30 min with stirring. Finally, the yellow GPd solution was gradually cooled to room temperature and was stored in a cold, dry, and dark place. This stock GPd solution was always used after sonication.

Instrumentation

Absorbance and UV–vis spectra were recorded using a Shimadzu(Japan) spectrophotometer (UV-1700) with 1.000-cm quartz cuvettes. Transmission electron microscopic (TEM) analyses were performed in a Hitachi(Japan) (H-9000 NAR) instrument on samples prepared by placing a drop of GPd solution on a Cu grid, precoated with carbon films, followed by solvent evaporation under vacuum. The GPd solution was centrifuged in a Heraeus(USA), Biofuge primo R machine and Fourier transform infrared spectroscopy (FTIR) data were collected using a Shimadzu(Japan) FT-IR 8400S spectrometer. The GPd solution was regularly sonicated in a Rivotek(India) ultrasonic bath (50 Hz) before any experimentation.

The buffer solutions were prepared following the literature method [50] and were measured with a Toshniwal(India) pH-meter (CL-54, India), calibrated as usual using standard buffers.

Kinetics

At ambient temperature and fixed ionic strength (μ = 1.0 M), in alkaline media (0.1–0.5 M NaOH) AO7 is reduced mainly to the corresponding amines, viz., 1-amino-2-napthol and sulfanilic acid [13,43,44] by sodium borohydride in the presence of GPd, whereas the uncatalyzed reduction of AO7 by sodium borohydride contributes nothing to the observed rate under similar reaction conditions (Fig. 1). Moreover, neither the GPd solution and/or aqueous gelatin solution (concentration $\leq$ 0.0075%) can reduce AO7, nor the addition of mere aqueous gelatin solution catalyzes the reduction of AO7 by borohydride. In both cases, the spectrum of AO7 does not change at least for 2 h. Thus it ensures that under the specified kinetic conditions, only in the presence of GPd nanoparticles, AO7 is reduced by borohydride and the gelatin molecules only acts as a stabilizing agent of the nanoparticles.

The reduction reaction was monitored spectrophotometrically following the change in the absorbance of the reaction mixture in situ in an electrically controlled thermostat. Kinetic data were measured at 485 nm where only AO7 shows absorption due to the presence of the color-generating chromophore (–N=N– group) [32]. The complete reduction of AO7 can thus be confirmed when the absorbance at 485 nm reaches

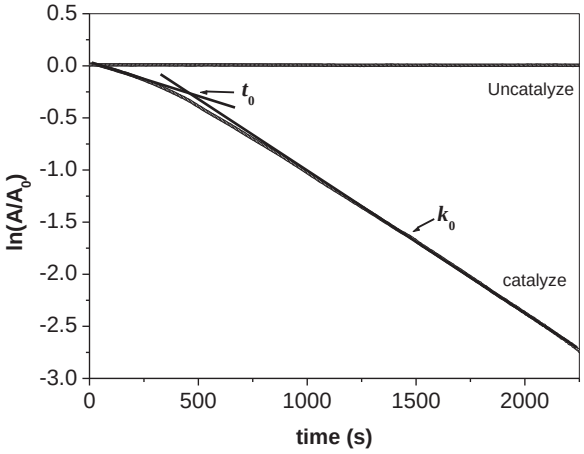

Figure 1 Plot of ln(A/A_0) versus time for uncatalyzed and GPd-catalyzed reduction of AO7, where A_0 and A are, respectively, the corresponding absorbance values at time zero and time t, measured at 485 nm. The catalyzed reduction follows a first-order kinetics (represented by the broken black line) with an induction period (t_0). Conditions: [AO7] = 0.05 mM, [$NaBH_4$] = 2.5 mM, [GPd] = 3.33×10^{-9} M, μ = 1.0 M, [NaOH] = 0.5 M, and $T = 25.0 \pm 0.1$°C.

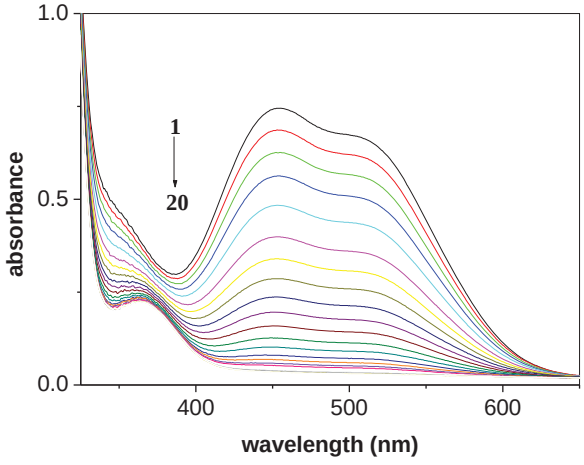

Figure 2 Spectral changes for the GPd nanoparticles-catalyzed reduction of AO7 by sodium borohydride at an interval of 2 min. Condition: [AO7] = 0.05 mM, [$NaBH_4$] = 10 mM, [GPd] = 3.33×10^{-9} M, μ = 1.0 M, [NaOH] = 0.5 M, *and* $T = 25.0 \pm 0.1$°C.

to a near-zero value (Fig. 2). Moreover, the reduction reactions of AO7 were performed in the presence of a large excess of borohydride over AO7. Usually, a reaction mixture was prepared by the successive addition of a measured amount of the GPd solution from the stock solution, sodium nitrate solution (to maintain the ionic strength, μ), and an alkaline solution of AO7 followed by the final quick addition of the borohydride

solution. The final volume of the reaction mixture was 3.0 mL. Linear, standard least-square fit to the derived first-order equation ($\ln(A/A_0) = -k_o t$ (where A_0 and A are the respective absorbance values of AO7 at time zero and time t) of the decay plot of absorbance with time yielded the observed first-order rate constants, k_o. Here, it should be mentioned that an initial time delay, i.e., an induction period (t_0) has been observed in the catalyzed reaction (Fig. 1), which was not considered in the determination of k_o values. The first point of time where the linear plots of $\ln(A/A_0)$ over the initial and subsequent experimental points intersects each other was taken as the induction time, t_0. The presence of the induction period does not arise due to the presence of aerial oxygen [51] or the impurities in the reaction medium since on passing argon or on addition of the chelating agent, like dipicolinic acid [52], the induction period remains as usual. This induction period originates from the inherent and adsorbate-induced surface restructuring of nanoparticles [53], which has been addressed later in detail. We assume that during this short period of time the adsorption of the reactants and the rate of the reduction reaction was yet to achieve full pace.

RESULTS AND DISCUSSION

Characterization of GPd

The formation of GPd was characterized by TEM imaging and UV–vis spectroscopy. The high-resoluttion transmission electron microscopy (HRTEM) images of the GPd are shown at two different magnifications in Fig. 3. High-resolution images show that most of the GPd nanoparticles are hexagonal, indicating a shell structure [54], and the diameter of a single nanoparticle was found to be about 4.5 nm.

Figure 4 presents the UV–vis spectra of aqueous solution of $PdCl_2$ and aqueous solution of GPd nanoparticles. The spectrum of GPd nanoparticles shows the absence of characteristic absorbance peaks of $PdCl_2$ at 235 and 413 nm, whereas the former one arises due to ligand-to-metal charge transfer transition [54–56]. Thus it can be logically assumed that Pd(II) ions have been mostly reduced to Pd(0) during the formation of nanoparticles.

The presence of gelatin molecules as the stabilizing agent on the nanoparticles' surface has been confirmed from the FTIR spectrum of GPd (Fig. 5). The FTIR spectrum of GPd was recorded after the centrifugation of the stock GPd solution (at 12,000 rpm for 30 min), followed by washing with Milli-Q water

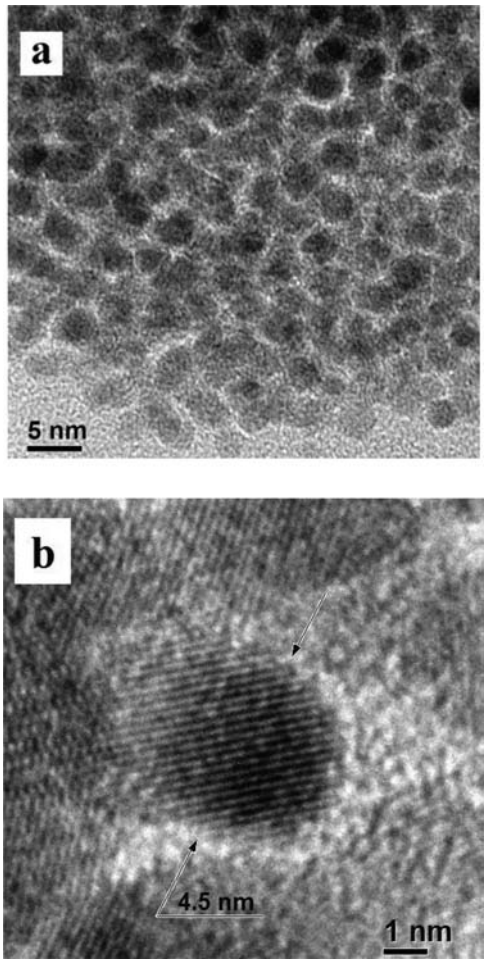

Figure 3 High-resolution transmission electron microscopy images of GPd nanoparticles (a) having an average diameter of nearly 4.5 nm (b).

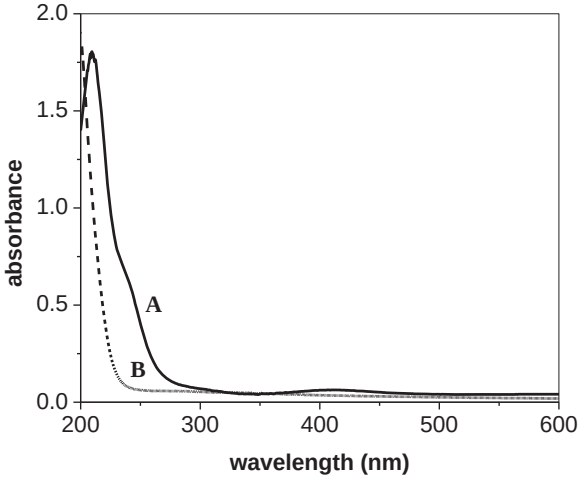

Figure 4 UV–vis spectra of aqueous solution of $PdCl_2$ (6.25×10^{-4} M) (A) and the aqueous solution of GPd nanoparticles (B).

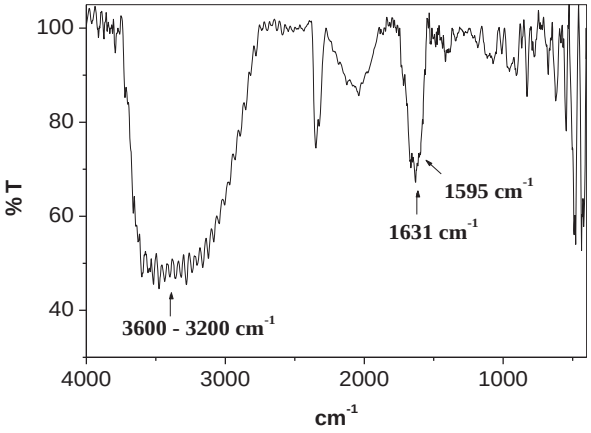

Figure 5 FTIR spectrum of GPd.

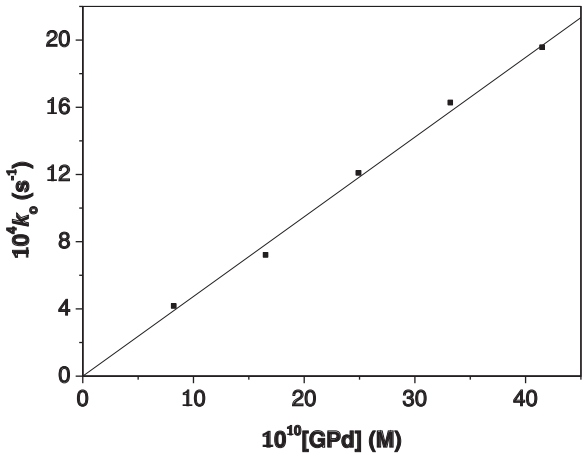

Figure 6 Observed rate, k_o of the catalyzed reduction of AO7 linearly increases with increasing concentration of GPd. Conditions: [AO7] = 0.05 mM, [$NaBH_4$] = 10 mM, μ = 1.0 M, [NaOH] = 0.5 M, and $T = 25.0 \pm 0.1$°C.

to remove excess gelatin. The main absorption bands at 1620 cm^{-1} (C=O stretching of amide) and 1595 cm^{-1} (N–H bending) arise due to the amide groups of gelatin molecules [57–59]. The spectrum confirms the presence of the gelatin molecule as the capping agent on the surface of Pd nanoparticles. Gelatin molecules generally have been found to attach itself electrostatically to the metal surface by their amine group [49,58,59].

Concentration of GPd

The HRTEM images show that the shapes of the GPd nanoparticles are mostly hexagonal with an estimated diameter of 4.5 nm (vide supra). Here, on the assumption that all the Pd(II) was reduced to Pd(0) and the nanoparticles are near spherical in shape with the same diameter as already mentioned, Eq. (1) gives an approximate concentration of GPd nanoparticles [60]:

$$[\text{GPd}] = [\text{Pd}^{2+}\text{ions}]/(V_{\text{GPd}}/V_{\text{Pd atom}}) \qquad (1)$$

where V refers to the corresponding volumes where the atomic radius of the Pd atom was taken as 0.137 nm [61]. The approximate concentration of stock GPd solution was calculated as 5.0×10^{-8} M, and the concentration of the GPd catalyst used in the reaction media is in the order of 10^{-10} M. Although the concentration of GPd is an rough estimate of the desired parameter but it serves the indispensable need in understanding the dependence of observed reaction rates on the GPd concentration and other factors.

Effect of [GPd] on k_o

The linear rise of the observed rate constant, k_o, with increasing [GPd] represents the general observation of the pseudo–first-order reaction (Fig. 6; Table S1 in the Supporting Information). The plot passes through the origin, which signifies that the reduction reaction between AO7 and borohydride happens only in the presence of the catalyst, and the contribution of the uncatalyzed reaction is negligible. Moreover, the plot ensures that the increasing gelatin concentration (0.0015–0.0075%) along with increasing [GPd] does not interfere with the reaction or passivate the catalyst in any way [53].

Effect of [AO7] and [$NaBH_4$] on k_o Values

Figures 7 and 8 describe the variation of k_o values with increasing [AO7] and [$NaBH_4$], respectively (Tables S2 and S3, respectively, in the Supporting Information). It can be seen that in both cases values of the k_o at first increase with the increase in [AO7] and [$NaBH_4$] reaching to an optimum value, then k_o decreases on a further increase in [AO7] and [$NaBH_4$].

The kinetic results firmly conclude that the reduction of AO7 by borohydride is a surface-catalyzed reaction where one or more reactants are adsorbed on the nanoparticle surface. Two kinetic models, viz., Eley–Rideal or by Langmuir–Hinshelwood mechanism, have been successfully employed to explain such surface reactions [62]. Here, since in both cases (Figs. 7 and 8) k_o shows similar behavior, it can be suggested

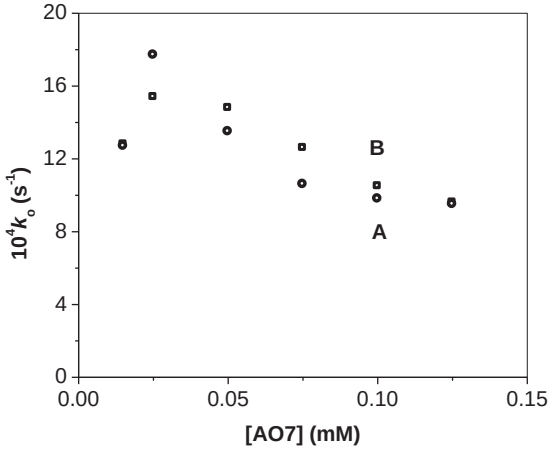

Figure 7 Variation of k_o values with [AO7]. Conditions: $[NaBH_4] = 2.5$ mM (A), 10 mM (B); [GPd] = 3.33 × 10^{-9} M; $\mu = 1.0$ M; [NaOH] = 0.5 M; $T = 25.0 \pm 0.1$°C.

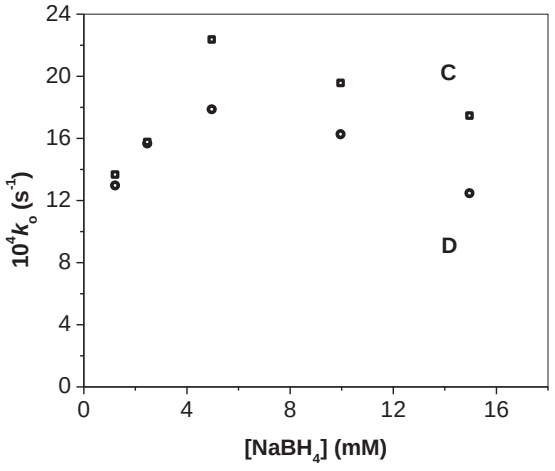

Figure 8 Variation of k_o values with [$NaBH_4$]. Conditions: [AO7] = 0.025 mM (C), 0.05 mM (D); [GPd] = 3.33 × 10^{-9} M; $\mu = 1.0$ M; [NaOH] = 0.5 M; $T = 25.0 \pm 0.1$°C.

that both the reactants AO7 and borohydride are adsorbed on the GPd surface and both the reactants compete with the same reaction sites [63–67]. Thus, in the presence of a certain amount of [GPd], when [AO7] or [$NaBH_4$] is increased, the reaction sites on the GPd surface are more occupied by the corresponding reactants and the rate also increases. But after reaching an optimum when the concentration of each reactant is further increased, that results in the occupation of reaction sites by only that reactant and the observed rate constants decreases due to the lack of other reactant ([$NaBH_4$] or [AO7], respectively).

The relative difference in the optimal concentration of AO7 and $NaBH_4$ after which k_o decreases,

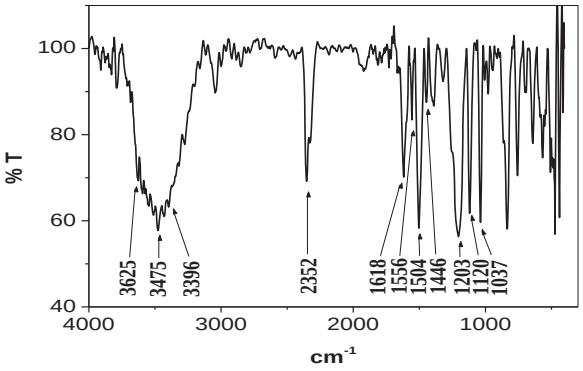

Figure 9 FTIR spectrum of pure AO7.

as displayed in Figs. 7 and 8, also needs an explanation. It can be seen that while the optimum concentration for AO7 lies around 0.025 mM, for $NaBH_4$ it is around 5 mM. A suitable account for this difference can be found in the disparity of the size of the reactants to be absorbed and the possible mode of adsorption.

The interaction of $NaBH_4$ with the metal nanoparticle surface had long been a subject of study. The interaction proceeds through several complex steps [68,69], and now it has been firmly established that ultimately the borohydride ion transfers a hydrogen species to the nanoparticle surface [63,64]. On the other hand, the interaction of AO7 with GPd can be followed by the change in the FTIR spectrum of pure AO7 and GPd–AO7 composite (Figs. 9 and 10, respectively).

The FTIR spectrum of pure AO7 shows several absorption bands, which are assigned as follows: 3060–3030 cm^{-1} (aromatic =C–H stretching), 1600–1450 cm^{-1} (aromatic C=C stretching), 1618 cm^{-1} (C=N stretching), 1556 cm^{-1} (related to NH–N=C grouping), 1504 cm^{-1} (N–H bending), 1446 cm^{-1} (N=N stretching), 1204 and 1120 cm^{-1} (coupling of SO_3^- stretching and aromatic =C–H bending), and 1037 cm^{-1} (C–OH stretching) [70–73].

Here, it is important to note that AO7 exists as an equilibrium between two tautomeric forms, viz., the azo form (A) and the hydrazone form (B) (Scheme 1) due to a rapid intramolecular proton exchange [73]. The presence of FTIR bands of AO7 at 1620 and 1446 cm^{-1} is in good agreement with the UV–vis spectrum of AO7 (Fig. 2). Figure 2 also shows two peaks at 430 and 485 nm, which supports the coexistence of both azo and hydrazone tautomeric forms of AO7, respectively [72,73].

The coexistence of both tautomeric forms is further supported by the absence of the FTIR band for carbonyl stretching of the pure azo form of AO7, which usually

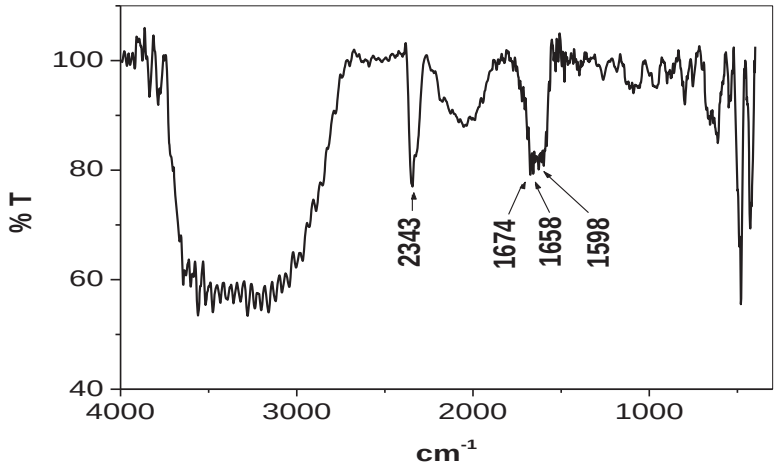

Figure 10 FTIR spectrum of the GPd–AO7 composite.

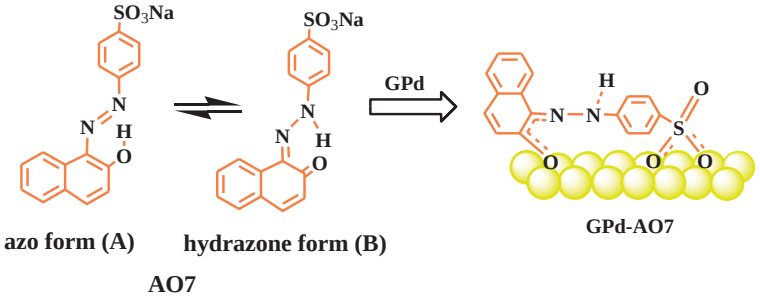

Scheme 1

appears at 1570 cm^{-1}. Owing to the delocalization of the H atom between oxygen and nitrogen atoms of AO7, a hydrazone tautomer is formed; and owing to the resulting intramolecular hydrogen bond (N–H–O), the double bond character of the carbonyl group is substantially reduced [72]. When AO7 is adsorbed on GPd, it can be seen that the FTIR bands at 1204 and 1120 cm^{-1} (SO_3^- stretching) and 1307 cm^{-1} (C–O–H stretching) have almost collapsed. On the basis of similar observation by Stylidi et al. and others [70,72], it can be assumed that AO7 is adsorbed on the GPd surface through the oxygen atom of the carbonyl group of the hydrazone form and two oxygen atoms of the sulfonate group (Scheme 1).

Since, an AO7 molecule with two phenyl groups is bulkier than the adsorbed hydrogen species, on adsorption AO7 molecules will cover up larger surface area than the other adsorbates. Thus on a small increase in [AO7], the surface tends to be more covered and the rate starts to decrease, whereas for a similar effect to take place for [$NaBH_4$] a relatively high concentration is required.

Effect of Media Alkalinity on k_o

The observed k_o values have been found to be decreasing with the increasing alkalinity of the reaction media (Fig. 11; Table S4 in the Supporting Information). Such a trend can be explained if the behavior of adsorbent GPd and AO7 and sodium borohydride in alkaline media is considered. With increasing alkalinity, borohydride ions are more stabilized and thus it is expected that a less number of hydride ions will be available on the catalyst surface, which in turn can have an effect on the decreasing rate. Moreover, AO7 in solution undergoes protolytic equilibria [74] as shown below:

$$L^{2-} + H^+ \overset{K_1}{\rightleftharpoons} LH^-, \quad K_1 = [LH^-]/[L^{2-}][H^+] \quad (2)$$

$$LH^- + H^+ \overset{K_2}{\rightleftharpoons} LH_2, \quad K_2 = [LH_2]/[LH^-][H^+] \quad (3)$$

The relative concentration of the three forms of AO7, viz., LH_2, LH^-, and L^{2-} depend on the pH of

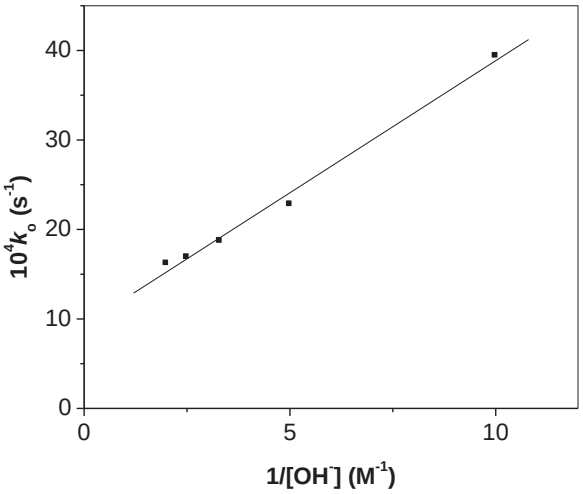

Figure 11 Variation of k_o versus 1/[OH^-]. Conditions: [AO7] = 0.05 mM, [$NaBH_4$] = 10 mM, [GPd] = 3.33 × 10^{-9} M, μ = 1.0 M, and $T = 25.0 \pm 0.1$°C.

the medium. The values of logarithm of the protonation constants K_1 and K_2 are 10.6 and 1.0 [75] which accounts for the deprotonation of naphthalene OH and SO_3H groups, respectively [76]. Thus, in 0.1–0.5 M NaOH media AO7 is mostly present as a doubly deprotonated L^{2-} form. Now, as the media alkalinity is increased, the palladium surface becomes more negative due to the enhanced interaction of the nanoparticles' surface with the OH^- ions [77]. Overall, an increase in media alkalinity results in the poor electrostatic attraction between the AO7 anion, the BH_4^- anion, and the negatively charged GPd surface. Thus, due to the lower extent of adsorption of AO7 and borohydride on GPd surface, the reaction rate is also diminished gradually [74–76].

Proposed Reaction Mechanism

Following the kinetic observations and the discussion described above, the catalyzed reaction steps are simply described in Scheme 2.

In step 1, the borohydride anions are adsorbed on the GPd surface to provide surface-adsorbed hydrogen species [63,64] and in step 2 AO7 molecules are adsorbed on the GPd surface. In step 3, AO7 is reduced to the corresponding amines, viz., 1-amino-2-napthol and sulfanilic acid, and then the products desorb from the GPd surface and the bare surface again takes part in the catalytic cycle. Steps 1 and 2 both are supposed to be reversible as they describe the fast adsorption or desorption processes, and step 3 is the rate-determining step [64].

The kinetic observations are best modeled by the Langmuir–Hinshelwood surface mechanism, and the rate of the reaction can simply be expressed as follows [63]:

$$\begin{aligned}\text{Rate} &= -\text{d[AO7]/dt} = k_o[\text{AO7}] \\ &= (kK_A[\text{AO7}]^\alpha K_B[\text{NaBH}_4]^\beta)/(1+K_A[\text{AO7}]^\alpha \\ &\quad + K_B[\text{NaBH}_4]^\beta)^2 \end{aligned} \quad (4)$$

where k is the true rate constant and K_A and K_B are the adsorption coefficients of AO7 and sodium borohydride, respectively. The exponents α and β are the corresponding reaction order in [AO7] and in [$NaBH_4$] [62], which has also been shown to be related to the heterogeneity of the nanoparticles surface [78].

If both $\alpha = \beta = 1$, then the above equation reduces to the classical Langmuir–Hinshelwood equation, which can be rearranged as [79]

$$\begin{aligned}&([\text{AO7}]/k_o[\text{AO7}])^{1/2} \\ &= (1 + K_B[\text{NaBH}_4])/(kK_AK_B[\text{NaBH}_4])^{1/2} \\ &\quad + [\text{AO7}](K_A/kK_B[\text{NaBH}_4])^{1/2} \end{aligned} \quad (5)$$

$$\begin{aligned}&\text{Or, } ([\text{NaBH}_4]/k_o[\text{AO7}])^{1/2} \\ &= (1+K_A[\text{AO7}])/(kK_AK_B[\text{AO7}])^{1/2} \\ &\quad + [\text{NaBH}_4](K_B/kK_A[\text{AO7}])^{1/2} \end{aligned} \quad (6)$$

Thus plots of $([\text{AO7}]/k_o[\text{AO7}])^{1/2}$ versus [AO7] and $([\text{NaBH}_4]/k_o[\text{AO7}])^{1/2}$ versus [$NaBH_4$] should be a straight line and indeed the plots have been found to be acceptably good straight lines (Figs. 12 and 13, respectively) [79].

Since the plots are linear and continuous, we can argue that the interaction between the adsorbate AO7 and the surface hydrogen species are relatively homogeneous. If the interaction had been heterogeneous, there would have been break in plots [53]. The observed continuous nature is further supported by the near constancy of the exponent values over the total reactant concentrations or in general at different molar ratios of [$NaBH_4$]/[AO7]. On the assumption that the adsorption of [AO7] and [$NaBH_4$] on the GPd surface is not so strong (since they are supposed to be reversible), Eq. (4) is reduced to

$$\text{Rate} = k_o[\text{AO7}] = kK_A[\text{AO7}]^\alpha K_B[\text{NaBH}_4]^\beta \quad (7)$$

$$\text{or,} \quad k_o = kK_A[\text{AO7}]^{\alpha-1} K_B[\text{NaBH}_4]^\beta \quad (8)$$

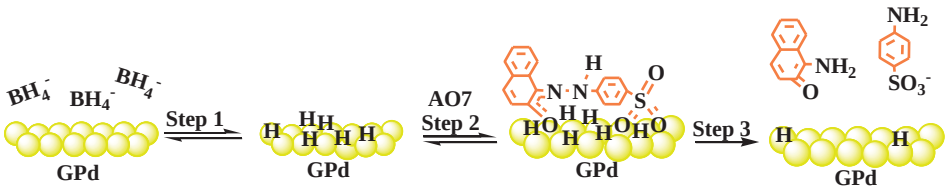

Scheme 2

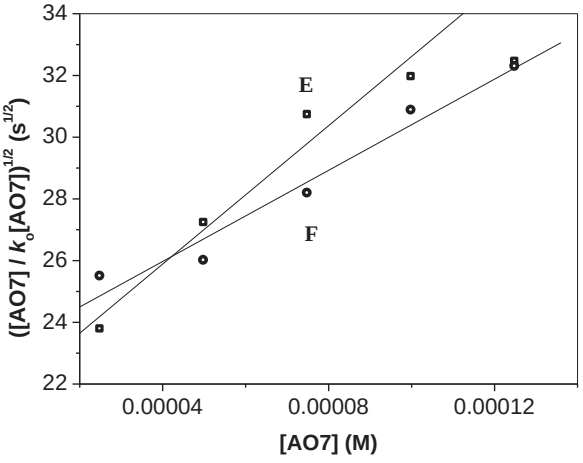

Figure 12 Plot of $([AO7]/k_o[AO7])^{1/2}$ versus [AO7]. Conditions: $[NaBH_4] = 2.5$ mM (E), 10 mM (F); $[GPd] = 3.33 \times 10^{-9}$ M; $\mu = 1.0$ M; [NaOH] = 0.5 M; and $T = 25.0 \pm 0.1$°C.

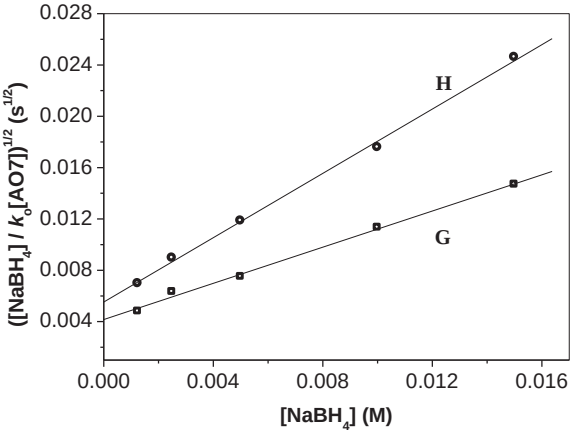

Figure 13 Plot of $([NaBH_4]/k_o[AO7])^{1/2}$ versus $[NaBH_4]$. Conditions: [AO7] = 0.025 mM (G), 0.05 mM (H); [GPd] $= 3.33 \times 10^{-9}$ M; $\mu = 1.0$ M; [NaOH] = 0.5 M; and $T = 25.0 \pm 0.1$°C.

The slopes of the plots of $\ln k_o$ versus ln[AO7] or $\ln k_o$ versus $\ln[NaBH_4]$ (Figs. 14 and 15, respectively) at the fixed concentration of other adsorbate ($NaBH_4$ or AO7, respectively) provide the corresponding exponent values with respect to the reactants [80]; numerical values of which are given in Table I. Both in Figs. 14 and 15, there is an increasing and decreasing linear segment, which signifies the mutual competition of the reactants toward the surface sites and consequently the variation in the reduction rate, k_o (vide supra). The mathematical signs of the exponent values indicate this variation in the rate (positive and negative signs correspond to the increasing and decreasing trends, respectively) and thus only the numerical values are considered.

It can be seen that the numerical values of α and β corresponding to the increasing and decreasing parts over different molar ratios are almost constant if we consider the error range. The variation in exponent values usually indicates the irregularity in the activation energy of the adsorption process [80]. Thus we can conclude that the interaction of the adsorbate molecules with the GPd surface is homogeneous.

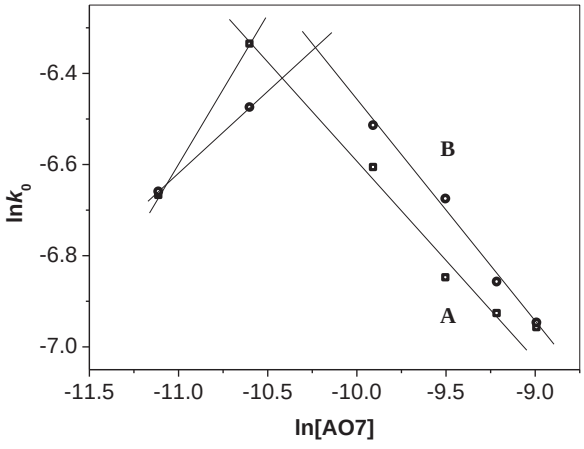

Figure 14 Plot of $\ln k_o$ versus ln[AO7]. Conditions: $[NaBH_4] = 2.5$ mM (A), 10 mM (B); $[GPd] = 3.33 \times 10^{-9}$ M; $\mu = 1.0$ M; [NaOH] = 0.5 M; and $T = 25.0 \pm 0.1$°C.

Moreover, if we relate the exponent values α and β to the reaction order, it can be said that the nature of mutual dependence of AO7 and adsorbed hydrogen species remains invariant on the change in the molar ratio. Since, for the reduction of the azo bond, each AO7

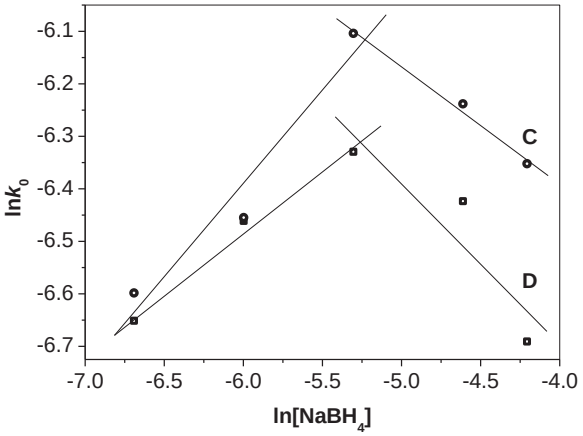

Figure 15 Plot of $\ln k_o$ versus $\ln[NaBH_4]$. Conditions: [AO7] = 0.025 mM (C), 0.05 mM (D); [GPd] = 3.33×10^{-9} M; μ = 1.0 M; [NaOH] = 0.5 M; and $T = 25.0 \pm 0.1$°C.

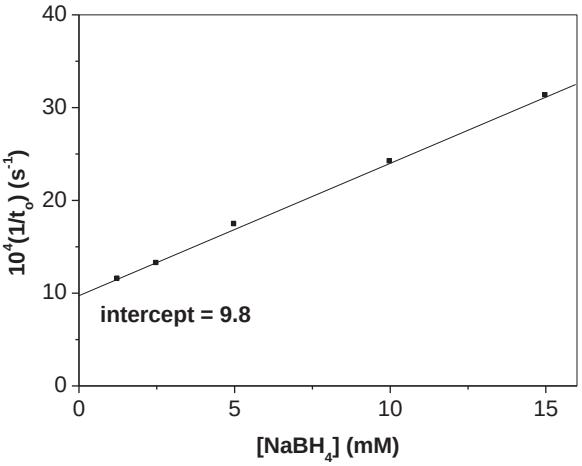

Figure 16 Plot of $1/t_0$ versus $[NaBH_4]$. Conditions: [AO7] = 0.05 mM, [GPd] = 3.33×10^{-9} M, μ = 1.0 M, [NaOH] = 0.5 M, and $T = 25.0 \pm 0.1$°C.

Table I Representative Values of Exponent α and β at Different Molar Ratios

	Exponent Value	Molar Ratio[a]	Exponent Value	Molar Ratio[a]
α^b	1.65	167–100	1.44 ± 0.03	50–22
α^c	1.36	667–400	1.48 ± 0.03	200–80
β^d	0.36 ± 0.08	50–200	0.22 ± 0.05	200–600
β^e	0.23 ± 0.02	25–100	0.31 ± 0.08	100–300

[a]Molar ratio = $[NaBH_4]/[AO7]$.

[b]$[NaBH_4] = 2.50$ mM, [GPd] = 3.33×10^{-9} M, μ = 1.0 M, [NaOH] = 0.5 M, and $T = 25.0 \pm 0.1$°C.

[c]$[NaBH_4] = 10.0$ mM, [GPd] = 3.33×10^{-9} M, μ = 1.0 M, [NaOH] = 0.5 M, and $T = 25.0 \pm 0.1$°C.

[d][AO7] = 0.025 mM, [GPd] = 3.33×10^{-9} M, μ = 1.0 M, [NaOH] = 0.5 M, and $T = 25.0 \pm 0.1$°C.

[e][AO7] = 0.05 mM, [GPd] = 3.33×10^{-9} M, μ = 1.0 M, [NaOH] = 0.5 M, and $T = 25.0 \pm 0.1$°C.

molecule needs four neighboring hydrogen species and the adsorbed hydrogen species are distributed over the nanoparticle surface, the reduction of the azo group successfully proceeds through a isotropic interaction and a single mechanistic pathway [81].

Role of Induction Period, t_0

The presence of an induction period, t_0, had been proposed to be a manifestation of the effect of surface restructuring of the GPd nanoparticles [63,65]. Since the atoms resting on the nanoparticle surface possess more potential energy than the atoms comprising the bulk of the particle, the surface always tends to reshuffle the atomic arrangement to lower the excess surface energy [82]. The rearrangement of the surface atoms usually results both from the spontaneous restructuring process and the adsorbate-induced process [82–84]. Nanoparticles, especially which are made up of the platinum group metals, due to relativistic effects, are more likely to go through this restructuring process [83]. The initial time period, $t_{0,}$ is thus a measure of extent of surface restructuring, and $1/t_0$ has been conceived as the rate of such a restructuring process [63,65]. The plot of $1/t_0$ versus $[NaBH_4]$ is shown in Fig. 16, which shows that the overall restructuring process increases with an increase in $[NaBH_4]$. At zero $[NaBH_4]$, the presence of an intercept value is particularly noteworthy, which actually represents the rate of occurrence of spontaneous restructuring ($1/t_{0,sp}$) [63,65]. Thus, the plot ($1/t_0 - 1/t_{0,sp}$) versus $[NaBH_4]$ (Fig. 17) describes the sole effect of adsorbate-induced restructuring of the surface, which passes through the origin and increases linearly with the increasing adsorbate concentration. If we plot $1/t_0$ against [GPd] (Fig. 18), naturally the plot passes through the origin, confirming that the nanoparticle surface is responsible for the presence of the induction period.

Effect of Temperature on Catalysis and Surface Restructuring

Both the rates of catalysis and the overall surface restructuring process increase with the increase in reaction temperature. The surface-restructuring energy and the activation energy of the GPd-catalyzed reduction of AO7 by $NaBH_4$ were evaluated from the plot of $\ln(1/t_0)$ versus $10^3/T$ and $\ln k_o$ versus $10^3/T$ (Figs. 19 and 20. respectively; Tables S5 and S6, respectively,

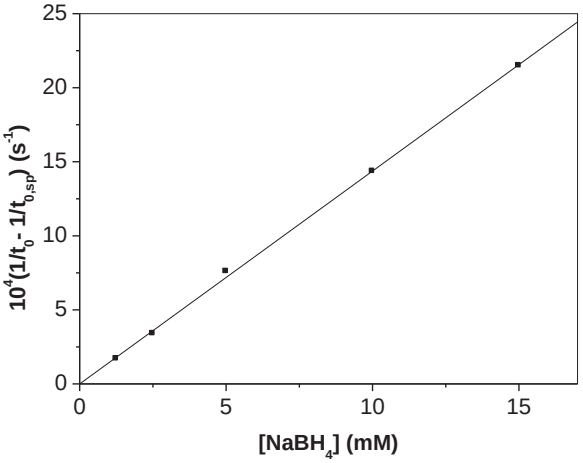

Figure 17 Plot of $(1/t_0 - 1/t_{0,sp})$ versus $[NaBH_4]$. Conditions: [AO7] = 0.05 mM, [GPd] = 3.33×10^{-9} M, μ = 1.0 M, [NaOH] = 0.5 M, and $T = 25.0 \pm 0.1$°C.

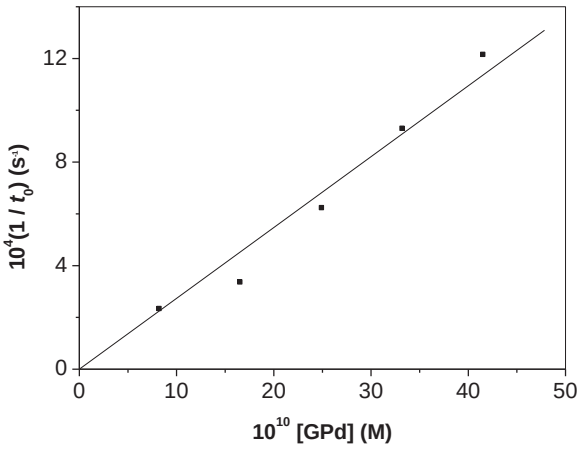

Figure 18 Plot of $1/t_0$ versus [GPd]. Conditions: [AO7] = 0.05 mM, $[NaBH_4]$ = 10.0 mM, μ = 1.0 M, [NaOH] = 0.5 M, and $T = 25.0 \pm 0.1$°C.

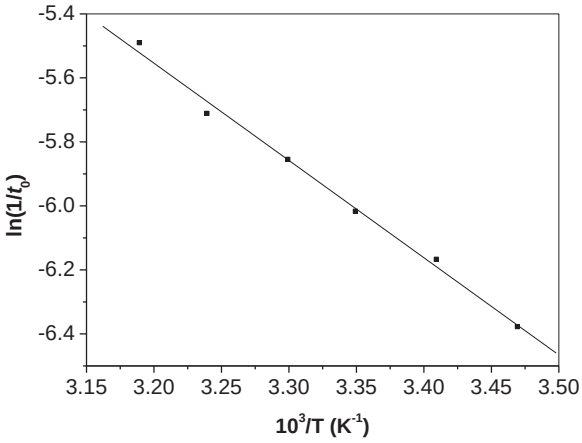

Figure 19 Plot of $\ln(1/t_0)$ versus $10^3/T$. Conditions: [AO7] = 0.05 mM, $[NaBH_4]$ = 10 mM, [GPd] = 3.33×10^{-9} M, μ = 1.0 M, and [NaOH] = 0.5 M.

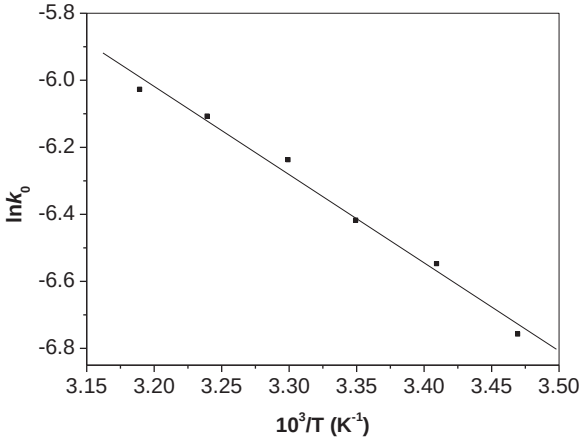

Figure 20 Plot of $\ln k_o$ versus $10^3/T$. Conditions: [AO7] = 0.05 mM, $[NaBH_4]$ = 10 mM, [GPd] = 3.33×10^{-9} M, μ = 1.0 M, and [NaOH] = 0.5 M.

in the Supporting Information) following the simple Arrhenius equation, $\ln k_o = \ln A - E_a/RT$, where k_o and A are the rate constant and the preexponential constant, respectively. From the slope of the corresponding plots, the calculated value of the surface-restructuring energy was found to be 25 ± 7 kJ M^{-1} and that of the activation energy, E_a was 22 ± 3 kJ M^{-1}, which is very close to that value as found earlier [63].

CONCLUSIONS

Well-characterized GPd nanoparticles were prepared by an one-pot synthesis method. A small amount of this GPd catalyzes the reduction of the harmful azo dye, AO7 by sodium borohydride in alkaline media. The reduction takes place on the GPd surface, and the kinetics follows the Langmuir–Hinshelwood kinetic model, where both AO7 and borohydride compete for the same surface site for adsorption on the GPd surface. The adsorption of AO7 is evident from the changes in the corresponding FTIR spectra. Detailed analysis also suggests that the reduction of AO7 by borohydride is isotropic over different molar ratios of [AO7]/$[NaBH_4]$. The presence of an induction period (t_0), which accounts for the surface-restructuring processes, emphasizes the crucial role of the nanoparticles surface in the catalyzed reaction.

The award of a senior research fellowship (Council for Scientific & Industrial Research, New Delhi, India) to R. S. Das is gratefully acknowledged.

BIBLIOGRAPHY

1. Travis, A. S. Technol Cult 1990, 31, 51–82.
2. Zollinger, H. Color Chemistry; VCH: Weinheim, Germany, 1991.
3. Christie, R. M. Colour Chemistry; Royal Society of Chemistry: Cambridge, UK, 2001.
4. Christie, R. M.; Mather, R. R.; Wardman, R. H. The Chemistry of Colour Application; Wiley-Blackwell: New York, 1999.
5. Bamfield, P. Chromic Phenomena, The Technological Applications of Colour Chemistry; The Royal Society of Chemistry: Cambridge, UK, 2001.
6. Herbst, W.; Hunger, K.; Wilker, G.; Ohleier, H.; Winter, R. Industrial Organic Pigments: Production, Properties, Applications; Wiley-VCH: Weinheim, Germany, 2004.
7. Maas, R.; Chaudhari, S. Process Biochem 2005, 40, 699–705.
8. Elisangela, F.; Andrea, Z.; Fabio, D. G.; Cristiano, R. M.; Regina, D. L.; Artur, C. P. Int Biodeterior Biodegradation 2009, 63, 280–288.
9. Stolz, A. Appl Microbiol Biotechnol 2001, 56, 69–80.
10. Gill, M.; Strauch, R. J.; Naturforsch, C. Z. J Biosci 1984, 39, 1027–1029.
11. Tsuboy, M. S.; Angeli, J. P. F.; Mantovani, M. S.; Knasmüller, S.; Umbuzeiro, G. A.; Ribeiro, L. R. Toxicol In Vitro 2007, 21, 1650–1655.
12. Golka, K.; Kopps, S.; Myslak, Z. W. Toxicol Lett 2004, 151, 203–210.
13. Pinheiro, H. M.; Touraud, E.; Thomas, O. Dyes Pigm 2004, 61, 121–139.
14. Shimada, C.; Kano, K.; Sasaki, Y. F.; Sato, I.; Tsuda, S. J Toxicol Sci 2010, 35, 547–554.
15. Zimmermann, T.; Kulla, G.; Leisinger, T. Eur J Biochem 1982, 129, 197–203.
16. Michaels, G. B.; Lewis, D. L. Environ Toxicol Chem 1985, 4, 45–50.
17. Pagga, U.; Brown, D.; Chemosphere 1986, 15, 479–491.
18. Anjaneyulu, Y.; Chary, N. S.; Rajk, D. S. S. Rev Environ Sci Biotechnol 2005, 4, 245–273.
19. Solísa, M.; Solísb, A.; Pérezb, H. I.; Manjarrezb, N.; Floresa, M. Process Biochem 2012, 47, 1723–1748.
20. Rai, H. S.; Bhattacharyya, M. S.; Singh, J.; Bansal, T. K.; Vats, P.; Banerjee, U. C. Environ Sci Technol 2005, 35, 219–238.
21. Zee, F. P. V.; Villaverde, S. Water Res 2005, 39, 1425–1440.
22. Chacko, J. T.; Subramaniam, K. Int J Environ Sci 2011, 1, 1250–1260.
23. Shi, B.; Li, G.; Wang, D.; Feng, C.; Tang, H. J Hazard Mater 2007, 143, 567–574.
24. Yang, C. L.; McGarrahan, J. J Hazard Mater 2005, 127, 40–47.
25. Ferrero, F.; Periolatto, M. Clean Technol Environ Policy 2012, 14, 487–494.
26. Srinivasan, A.; Viraraghavan, T. J Environ Manage 2010, 91, 1915–1929.
27. Demirbas, A. J Hazard Mater 2009, 67, 2009 1–9.
28. Mahmoodi, N. M.; Arami, M. J Photochem Photobiol B 2009, 94, 20–24.
29. Comparelli, R.; Fanizza, E.; Curri, M. L.; Cozzoli, P. D.; Mascolo, G.; Agostiano, A. Appl Catal B 2005, 60, 1–11.
30. Singh, K.; Arora, S. Environ Sci Technol 2011, 41, 807–878.
31. Lodha, B.; Chaudhari, S. J Hazard Mater 2007, 148, 459–466.
32. Ramirez, J. H.; Cost, C. A.; Madeira, L. M. Catal Today 2005, 107–108, 68–76.
33. Ramirez, J. H.; Vicente, M. A.; Madeira, L. M. Appl Catal B 2010, 98, 10–26.
34. Pintar, A. Catal Today 2003, 77, 451–465.
35. Donlagicä, J.; Levec, J. Environ Sci Technol 1998, 32, 1294–1302.
36. Nishide, S.; Shoda, M. Energy Environ Res 2012, 2, 1–12.
37. Mielczarski, J. A.; Atenas, G. M.; Mielczarski, E. Appl Catal B 2005, 56, 289–303.
38. Bokare, A. D.; Chikate, R. C.; Rode, C. V.; Paknikar, K. M. Appl Catal B 2008, 79, 270–278.
39. Bokare, A. D.; Chikate, R. C.; Rode, C. V.; Paknikar, K. M. Environ Sci Technol 2007, 241, 7437–7443.
40. Peng, Y.; Fu, D.; Liu, R.; Zhang, F.; Liang, X. Chemosphere 2008, 71, 990–997.
41. Zhang, C.; Zhu, Z.; Zhang, H.; Hu, Z. J Environ Sci 2012, 24, 1021–1026.
42. Zhang, G.; Qu, J.; Liu, H.; Cooper, A. T.; Wu, R. Chemosphere 2007, 68, 1058–1066.
43. Straub, R. F.; Voyksner, R. D.; Keever, J. T. Anal Chem 1993, 65, 2131–2136.
44. Xu, L.; Wu, X. C.; Zhu, J. J Nanotechnol 2008, 19, 1–6.
45. Molnar, A. Chem Rev 2011, 111, 2251–2320.
46. Bradley, J. S. In Clusters and Colloids; Schmid, G., Ed.; VCH: Weinheim, Germany, 1994.
47. Shutava, T. G.; Balkundi, S. S.; Vangala, P.; Steffan, J. J.; Bigelow, R. L.; Cardelli, J. A.; O'Neal, D. P.; Lvov, Y. M. ACS Nano 2009, 3, 1877–1885.
48. Neupane, M. P.; Lee, S. J.; Park, I. S.; Lee, M. H.; Bae, T. S.; Kuboki, Y.; Uo, M.; Watari, F. J Nanopart Res 2011, 13, 491–498.
49. Liu, Y.; Liu, X.; Wang, X. Nanoscale Res Lett 2011, 6, 22–33.
50. Perrin, D. D.; Demsey, B. In Buffers for pH and Metal Ion Control; Chapman and Hall: London, 1974.
51. Sharma, G.; Ballauff, M. Macromol Rapid Commun 2004, 25, 547–555.
52. Das, R. S.; Singh, B.; Mukhopadhyay, S.; Banerjee, R. Dalton Trans 2012, 41, 4641–4648.
53. Das, R. S.; Singh, B.; Banerjee, R.; Mukhopadhyay, S. Dalton Trans 2013, 42, 4068–4080.

54. Teranishi, T.; Miyake, M. Chem Mater 1998, 10, 594–600.
55. Li, Y.; Hong, X. M.; Collard, D. M.; El-Sayed, M. A. Org Lett 2000, 2, 2385–2388.
56. Redon, R.; Rendon-Lara, S. K.; Fernandez-Osorio, A. L.; Ugalde-Saldivar, V. M. Rev Adv Mater Sci. 2011, 27, 31–42.
57. Liu, S.; Zhang, Z.; Han, M. Y. Adv Mater 2005, 17, 1862–1866.
58. Gaihrea, B.; Khil, M. S.; Lee, D. R.; Kim, H. Y. Int J Pharm 2009, 365, 180–189.
59. Neupane, M. P.; Lee, S. J.; Park, I. S.; Lee, M. H.; Bae, T. S.; Kuboki, Y.; Uo, M.; Watari, F. J Nanopart Res 2011, 13, 491–498.
60. Narayanan, R.; El-Sayed, M. A. J Phys Chem B 2003, 107, 12416–12424.
61. Greenwood, N. N.; Earnshaw, A. In Chemistry of the Elements, 2nd ed.; Butterworth–Heinemann: Oxford, UK, 1997.
62. Long, J.; Xie, X.; Xu, J.; Gu, Q.; Chen, L.; Wang, X. ACS Catal 2012, 2, 622–631.
63. Wunder, S.; Polzer, F.; Lu, Y.; Mei, Y.; Ballauff, M. J Phys Chem C 2010, 114, 8814–8820.
64. Wunder, S.; Lu, Y.; Albrecht, M.; Ballauff, M. ACS Catal 2011, 1, 908–916.
65. Kaiser, J.; Leppert, L.; Welz, H.; Polzer, F.; Wunder, S.; Wanderka, N.; Albrecht, M.; Lunkenbein, T.; Breu, J.; Kummel, S.; Lu, Y.; Ballauff, M. Phys Chem Chem Phys 2012, 14, 6487–6495.
66. Zhou, X.; Xu, W.; Liu, G.; Panda, D.; Chen, P. J Am Chem Soc 2010, 132, 138–146.
67. Han, K. S.; Liu, G.; Zhou, X.; Medina, R. E.; Chen, P. Nano Lett 2012, 12, 1253–1259.
68. Liu, B. H.; Li, Z. B. J Power Sources 2009, 187, 527–534.
69. Guella, G.; Patton, B.; Miotello, A. J Phys Chem C 2007, 111, 18744–18750.
70. Stylidi, M.; Kondarides, D. I.; Verykios, X. E. App Catal B 2004, 47, 189–201.
71. Stylidi, M.; Kondarides, D. I.; Verykios, X. E. Appl Catal B 2003, 40, 271–286.
72. Bauer, C.; Jacques, P.; Kalt, A. Chem Phys Lett 1999, 307, 397–406.
73. Zhang, S.; Yu, H.; Li, Q. Chemosphere 2005, 61, 1003–1011.
74. Bourikas, K.; Stylidi, M.; Kondarides, D. I.; Verykios, X. E. Langmuir 2005, 21, 9222–9230.
75. Abramian, L.; El-Rassy, H. Chem Eng J 2009, 150, 403–410.
76. Li, G.; Qua, J.; Zhang, X.; Liu, H.; Liu, H. J Mol Catal A: Chem 2006, 259, 238–244.
77. Konstantinou, I. K.; Albanis, T. A. Appl Catal B 2004, 49, 1–14.
78. Laszlo, K.; Podkoscielny, P.; Daborwski, A. Langmuir 2003, 19, 5287–5294.
79. Rajaram, J.; Kuriacose, J. C. Kinetics and Mechanisms of Chemical Transformations; Macmillan India: New Delhi, India , 2011.
80. Wong, Y. C.; Szeto, Y. S.; Cheung, W. H.; McKay, G. Langmuir 2003, 19, 7888–7894.
81. Kang, H. C.; Weinberg, W. H. Chem Rev 1995, 95, 667–676.
82. Titmuss, S.; Wander, A.; King, D. A. Chem Rev 1996, 96, 1291–1305.
83. Kiskinova, M. Chem Rev 1996, 96, 1431–1447.
84. Somorjai, G. A.; Rupprechter, G. J Chem Educ 1998, 75, 161–176.